SS-Detect: Development and Validation of a New Strategy for Source-Based Morphometry in Multi-Scanner Studies

Ruiyang Ge [a,*], Shiqing Ding [a], Tyler Keeling [a],

William G. Honer [b], Sophia Frangou [b,c], Fidel Vila-Rodriguez [a]

[a] Non-Invasive Neurostimulation Therapies Laboratory, Department of Psychiatry, University of British Columbia, BC, Canada

[b] Department of Psychiatry, University of British Columbia, BC, Canada

[c] Department of Psychiatry, Icahn School of Medicine at Mount Sinai, NY, USA

* Correspondence to: Ruiyang Ge, PhD

Non-Invasive Neurostimulation Therapies Laboratory, Department of Psychiatry, University of British Columbia, 2255 Wesbrook Mall, Vancouver, BC, Canada

E-mail: ruiyang.ge@ubc.ca OR ruiyangge@hotmail.com

Running Title: A simulation study of source-based morphometry analysis strategies

Keywords: simulation; source-based morphometry; structural brain pattern; T1-weighted MRI

Acknowledgements and Disclosure: We sincerely thank the study participants and MRI technologists at the UBC MRI Research Centre. RG, SD, TK, and SF declare no potential conflict of interest with respect to the research, authorship, and/or publication of this article. Dr. Honer has received consulting fees or sat on paid advisory boards for: AlphaSights, Guidepoint, In Silico, Translational Life Sciences, Otsuka, Lundbeck, and Newron, and holds shares in Translational Life Sciences and Eli Lilly. FVR reports research grants from CIHR, Brain Canada, Michael Smith Foundation for Health Research, and Vancouver Coastal Health Research Institute; reports receiving in-kind equipment support for this investigator-initiated trial from MagVenture; and consulting honoraria from Janssen pharmaceutical.

ABSTRACT (246 words)

Background and Purpose: Source-based morphometry (SBM) is a data-driven multivariate approach for interrogating covariation in structural brain patterns (SBPs) across subjects and quantifying the subject-specific loading parameters of these patterns. This approach has been used in multi-centre studies pooling magnetic resonance imaging (MRI) data across different scanners to advance the reproducibility of neuroscience research. In the present study, we developed an analysis strategy for Scanner-Specific Detection (SS-Detect) of SBPs in multi-scanner studies, and evaluated its performance relative to a conventional strategy.

Methods: We conducted two simulation experiments. In the first experiment, the SimTB toolbox was used to generate simulation datasets mimicking twenty different scanners with common and scanner-specific SBPs. In the second experiment, we generated one simulated SBP from empirical datasets from two different scanners.

Results: The outputs of the conventional strategy were limited to whole-sample-level results across all scanners; the outputs of SS-Detect included whole-sample-level and scanner-specific results. In the first simulation experiment, SS-Detect successfully estimated all simulated SBPs, including the common and scanner-specific SBPs whereas the conventional strategy detected only some of the whole-sample SBPs. The second simulation experiment showed that both strategies could detect the simulated SBP. Quantitative evaluations of both experiments demonstrated greater accuracy of the SS-Detect in estimating spatial SBPs and subject-specific loading parameters.

Conclusions: SS-Detect outperformed the conventional strategy in terms of accurately estimating spatial SBPs and loading parameters both at whole-sample and scanner-specific levels and can be considered advantageous when SBM is applied to a multi-scanner study.

1. INTRODUCTION

Source-based morphometry (SBM) is a data-driven multivariate approach for identifying cross-subject covarying structural brain patterns (SBPs) and the subject-specific loading parameters of these patterns.[1, 2] While this approach was initially proposed as an extension to voxel-based morphometry of gray matter volume (GMV),[3] it has also been implemented to construct SBPs based on cortical thickness,[4] myelin volume fraction,[5] and fractional anisotropy.[6]

To date, SBM has been predominantly used in single-scanner studies to investigate neuroanatomical differences between populations and neuroanatomical correlates of demographic or clinical characteristics.[7-10] More recently, SBM has also been employed in collaborative studies,[11-14] since pooling of multi-scanner magnetic resonance imaging (MRI) data from multiple sites has gained research momentum in the past decade.[15, 16] Theoretically, SBM assumes common SBPs and varying loading parameters across all subjects of the investigated cohort.[1, 3] Therefore, the conventional strategy to implement SBM in a multi-scanner setting is to directly concatenate data from the different scanners to form a single matrix as the input of independent component analysis (ICA);[3] the outputs are whole-sample-level SBPs derived from the entire study sample across all scanners. The main limitations of this strategy is that it only yields whole-sample-level SBPs and it cannot ascertain scanner-specific variations. There is growing interest in studying individual variability in neuroscience,[17, 18] but the data-pooling nature of current SBM techniques precludes personalized SBPs detection.[2] To align SBM with the goal of precision neuroscience, it is vital that we develop new ways to model scanner-specific SBPs, and infer more accurate estimates of subject-specific loading parameters. To address this challenge, we developed SS-Detect, a novel analysis strategy to detect scanner-specific structural brain patterns in multi-scanners studies and used simulation experiments to evaluate its performance against the conventional strategy.

2. METHODS

2.1 SBM analysis strategies for multi-scanner studies

The conventional SBM analysis method for a multi-scanner study concatenates all the data from the different scanners to form a single matrix as the input for further analyses (Figure 1A). In this case $\mathbf{X}'_{\mathbf{wholesample}} = [\mathbf{x_1}; \mathbf{x_2}; \ldots; \mathbf{x_n}]$ would be a typical data matrix, where $\mathbf{x}_i$ is the data matrix from the i-th scanner with dimension of $i_n \times v$, in which i_n is the n-th subject studied on the i-th scanner and v represents voxel number. Principal component analysis (PCA) is performed on $\mathbf{X}'_{\mathbf{wholesmaple}}$ for dimensional reduction across all subjects scanned across all scanners. Thereafter, ICA is performed on $\mathbf{X}_{\mathbf{wholesample}}$ which is the reduced data matrix, and the outputs

of ICA are the whole-sample-level SBPs ($\mathbf{S}_{\mathbf{wholesample}}$) and their associated loading parameter matrix ($\mathbf{A}_{\mathbf{wholesample}}$).

Figure 1B presents the flowchart of the SS-Detect which is a scanner-specific analysis strategy. By analogy to the group ICA approach used in functional MRI studies,[19] SS-Detect first applies PCA to data matrix $\mathbf{x}_i, i \in [1, \mathrm{n}]$, then a second PCA procedure is conducted on the concatenated matrix $\boldsymbol{X}'_{\mathbf{wholesample}}$ which is followed by the ICA procedure to obtain the whole-sample-level SBP matrix $\mathbf{S}_{\mathbf{wholesample}}$ and loading parameter matrix $\mathbf{A}_{\mathbf{wholesample}}$. The final step is to back-reconstruct the scanner-specific-level results based on the whole-sample-level results and PCA compression and projection.[20]

2.2 Simulation with SimTB toolbox

We evaluated and compared the conventional and the SS-Detect strategies with GMV data from simulated structural MRI data. Although GMV was used as an exemplar the method can be implemented using other structural metrics (e.g. cortical thickness). We generated 20 GMV datasets mimicking 20 different scanners using the SimTB toolbox.[21, 22] In simulated data representing each scanner, the number of subjects was randomly generated between 50 and 100. Simulated data representing each scanner were generated as the product of a loading parameter matrix and a SBP matrix. The code used to generate simulated data is available on GitHub (https://github.com/ruiyangge/multiscanner_SBM). The first 10, and second 10 datasets were comprised of 15 SBPs each (with dimension 300×300 with baseline intensity of 1,000). The two sets of 10 datasets shared 14 common SBPs, yielding 16 different SBPs in total. The two dataset-specific SBPs were generated to mimic the variability of SBPs between different scanners. Spatial locations of these 16 SBPs are shown in Figure 2A. Rician noise was added to the simulated datasets with different signal-to-noise-ratio (SNR, uniformly varied from 40 to 110),[23, 24] defined as $\bar{S}/\sigma_N$, where $\bar{S}$ is the mean value of the SBP signal and σ_N is the standard deviation of the noise. Varying SNR values were used to mimic the varying distribution of SNR values across different scanners.[25] Then, the conventional and the proposed analysis strategies were then applied to these 20 datasets, with model orders of ICA were set as 16 for both strategies. To test the stability of the ICA decomposition, the ICASSO technique with one-hundred ICA repetitions was used.[26]

2.3 Simulation with empirical GMV data

In this simulation, we used two datasets collected at the University of British Columbia MRI Research Centre on a Philips Achieva 3.0-T scanner and a GE Genesis Signa 1.5-T scanner. Each dataset comprised 43 healthy participants (25 females). The age range of the participants

was 18-63 and 16-47 years, for the Philips and GE datasets respectively. All participants provided written informed consent and studies were approved by the University of British Columbia ethics board. T1-weighted images from the Philips Achieva scanner were acquired with the following parameters: 165 axial slices; TR = 8.1 ms; TE = 3.5 ms; flip angle (FA) = 8°; field of view (FOV) = 256 mm×256 mm×165 mm; acquisition matrix= 256×250; slice thickness = 1 mm. T1-weighted images from the GE Genesis Signa scanner were acquired with the following parameters: 124 axial slices; TR = 11.2 ms; TE = 2.1 ms; FA= 20°; FOV = 256 mm× 256 mm×260 mm; acquisition matrix= 256×256; slice thickness = 1.5 mm.

Preprocessing for voxel-based morphometry was performed using the CAT12 toolbox (http://www.neuro.uni-jena.de/cat/). First, the images were segmented into gray matter, white matter and cerebrospinal fluid probability maps by unified segmentation. Next, gray matter images were registered to the tissue probability map using affine transformation. Diffeomorphic Anatomical Registration using Exponential Lie Algebra was carried out to implement a high-dimensional nonlinear normalization. Through iteration of image registration and template creation, gray matter maps were normalized to their own average templates and further to the Montreal Neurological Institute space, and resampled to a voxel size of 1.5 mm^3. Thereafter, normalized gray matter images were modulated with the Jacobian determinants of the nonlinear transformation and smoothed with an 8 mm^3 Gaussian kernel. After pre-processing, we obtained normalized, modulated, and smoothed GMV images for subsequent SBM analysis.

We first decomposed each dataset into 10 SBPs with SBM, and replaced one randomly-selected empirical SBP with a simulated SBP located in the frontal lobe (Figure 4A). Specifically, data for the background voxels (voxels outside of the selected frontal region) were randomly generated with the MATLAB “randn” function, and data of the SBP voxels were drawn from the empirical SBP. The loading parameter matrix was randomly generated with the “randn” function. Simulated MRI data of each dataset were generated as the product of the loading parameter matrix and the SBP matrix. Thereafter, the conventional SBM analysis strategy, and the proposed strategy for multi-scanner studies were applied to the simulated datasets, with the model orders of ICA set as 10 for each strategy. This procedure was repeated ten times, with the ICASSO technique using one-hundred ICA repetitions in each run.

2.4 Evaluation of the two strategies

Three quantitative measures were used to assess the two analysis strategies: (1) Dice’s coefficients between spatial templates and SBPs; (2) area under curve (AUC) of the curves of

Dice's coefficients; and (3) Pearson's correlation coefficients between ground-truth loading vectors and estimated loadings.

In the SimTB-based simulated data, overall performance at the whole-sample-level results was the mean of each quantitative measure across the 16 SBPs; overall performance at the scanner-specific results was the mean of each quantitative measure across the 15 simulated SBPs for the first 10 and the second 10 datasets, respectively.

In the empirical data-based simulation, overall performance both at the whole-sample-level and the scanner-specific results was the final value of each performance measure averaged across ten runs.

Finally, we compared the performance measures (i.e., Dice's coefficients, AUC of Dice's coefficient's curve, and correlation coefficients of loadings) between the two analysis strategies with Wilcoxon signed-rank tests. The statistical significance level was set as $p < 0.05$.

2.4.1 Evaluation of the whole-sample-level spatial SBPs

The whole-sample-level spatial SBPs could be detected with both analysis strategies. For each experiment, we computed the Dice's coefficients between the ground-truth templates (see Figure 2A, and Figure 4A) and the SBPs. Dice's coefficient ranges from 0 to 1, with higher values indicating higher similarity between two binary images. We first z-transformed the SBPs, then used a z-threshold to binarize the SBPs, varying this threshold over an interval of [0.1, 10]. We took the Dice's coefficient with z-threshold = 2.5 as one quantitative measure of the analysis strategies, this z-threshold was selected because it is an popular empirical threshold for displaying the results of spatial SBPs.[12, 27-29] We also plotted curves of the Dice's coefficients with varying z-thresholds, and computed the area under curve (AUC) as another quantitative measure.

*2.4.2 Evaluation of the scanner-*specific *spatial SBPs*

The scanner-specific spatial SBPs could be detected only with SS-Detect. For the scanner-specific spatial SBPs of the SimTB data, we used a one-sample t-test to summarize the results of the first 10 and second 10 datasets separately, and used t-thresholds varying between 0.1 and 10 to binarize the t-maps.

For the scanner-specific spatial SBPs of the empirical data, we used a one-sample t-test to summarize the results of Philips and GE data separately, with t-thresholds varying between 0.1 and 75 to binarize the t-maps. Dice's coefficient between the thresholded t-maps and ground-truth templates at each t-threshold was then computed.

2.4.3 Evaluation of the loadings of the SBPs

Each subject had a single loading parameter for each SBP. To assess the detection ability of the analysis strategies for the loading parameters, we computed the Pearson's correlations between the ground-truth loading vectors and those obtained from each strategy. This procedure was the same for both experiments.

RESULTS

Results from the simulated datasets

Figure 2 presents the estimated SBPs based on the two analysis strategies. At the whole-sample-level, the SS-Detect successfully detected all 16 simulated SBPs (Figure 2C), whereas the conventional analysis detected only 12 as some SBPs were apparently fused (Figure 2B); for example, one estimated SBP (pattern ID: 1, Figure 2B) consisted of two simulated SBPs (pattern IDs: 1 and 11, Figure 2A). SS-Detect successfully detected both the 14 common and the 2 scanner-specific SBPs in each scanner-specific dataset and at the whole-sample-level. The results of the first 10 datasets contained a "noise-like" SBP (pattern ID: 16) which was not simulated in these datasets, and the results of the second 10 datasets contained a "noise-like" SBP (pattern ID: 15) which was not simulated in these datasets.

Quantitative evaluation of the SBM results showed that at the whole-sample-level, estimated SBPs from the SS-Detect had higher AUC and Dice's coefficient (z-score = 2.5) relative to the conventional analysis (Figure 3A). Although the first 10 simulated datasets had different SBPs compared with the second 10 datasets, their AUC and Dice's coefficients were similar (Figure 3B). Figure 3C shows that the average correlation coefficient between the estimated loading parameters and the ground-truth loadings from SS-Detect was significantly higher than that from the conventional strategy. This finding was detected both in the first 10 datasets (MEAN±SE: 0.828±0.008 versus 0.745±0.026) and the second 10 datasets (MEAN±SE: 0.841±0.006 versus 0.731±0.028).

Results from empirical data

At the whole-sample level, SS-Detect successfully estimated the simulated SBP (Figure 4C), whereas the estimated SBP from the conventional strategy included regions (e.g., right superior parietal regions) which were not part of the SBP (Figure 4B). Therefore, the conventional strategy detected false-positive regions. Quantitative evaluation of the SBM results showed that at the whole-sample-level, SS-Detect estimated SBPs with higher AUC and Dice's coefficient (z-score = 2.5) relative to the conventional analysis (Figure 5A). At the scanner level, SS-Detect successfully detected the simulated SBP for both datasets (Figure 4D). The AUC of the Philips dataset was slightly higher than that of the GE dataset (Figure 5B). Figure 5C shows that the

average correlation coefficient between the estimated loading parameters and the ground-truth loadings from SS-Detect was significantly higher than that from the conventional strategy. This finding was observed in both in MRI data from Philips Achieva scanner (MEAN±SE: 0.878±0.022 versus 0.728±0.057) and GE Genesis Signal scanner (MEAN±SE: 0.895±0.017 versus 0.804±0.050).

DISCUSSION AND CONCLUSIONS

In this paper, we proposed SS-Detect as a scanner-specific analysis strategy to improve the detection of SBPs in SBM analyses of multi-scanner datasets. SS-Detect can be considered an adaptation to anatomical MRI studies of the commonly-used group ICA in the field of functional MRI.[19, 30] Both SS-Detect and the conventional strategy assessed in the present study employed group ICA to establish correspondence of SBPs across datasets acquired with different MRI scanners. The present report describes a simulation study to assess the performance of SS-Detect. Firstly, qualitative visualization showed that SS-Detect could successfully estimate all SBPs, both at the whole-sample-level and at the individual scanner-level. These findings suggest that SS-Detect preserves the variability of the SBPs between different scanners, which cannot be ascertained with the conventional strategy. Secondly, quantitative comparisons in two experiments demonstrated that SS-Detect was more accurate than the conventional strategy in estimating both the SBPs and subject-specific loading parameters. These findings underscore the advantage of using SS-Detect for analysis of SBM in a multi-scanner study.

Future studies will be necessary to extend this work in two ways. First, SS-Detect could be used to explore systematic differences introduced into a multi-scanner MRI study because of the different scanning platforms used; this could also assist in eliminating undesired noise which confounds true effects of interest.[31, 32] Second, relative to the conventional analysis strategy, SS-Detect is a further step towards the goal of precision neuroscience by establishing correspondence of SBPs in the entire study sample across scanners and simultaneously preserving the variability within each scanner-specific dataset. Nonetheless, the primary limitation of SS-Detect is that it cannot be applied at an individual subject level. Accordingly, future studies are need to go beyond, by addressing individual subject variability. Constructing SBPs from an individual anatomical MRI image would make it possible to investigate variability between individuals.[2, 33]

REFERENCES

[1] Gupta CN, Turner JA, Calhoun VD. Source-based morphometry: a decade of covarying structural brain patterns. *Brain Structure and Function*. 2019:1-14.

[2] Alexander-Bloch A, Giedd JN, Bullmore E. Imaging structural co-variance between human brain regions. *Nature Reviews Neuroscience*. 2013;14:322-36.

[3] Xu L, Groth KM, Pearlson G, Schretlen DJ, Calhoun VD. Source‐based morphometry: The use of independent component analysis to identify gray matter differences with application to schizophrenia. *Human brain mapping*. 2009;30:711-24.

[4] Steenwijk MD, Geurts JJ, Daams M, Tijms BM, Wink AM, Balk LJ, Tewarie PK, Uitdehaag BM, Barkhof F, Vrenken H. Cortical atrophy patterns in multiple sclerosis are non-random and clinically relevant. *Brain*. 2016;139:115-26.

[5] O'Muircheartaigh J, Dean III DC, Ginestet CE, Walker L, Waskiewicz N, Lehman K, Dirks H, Piryatinsky I, Deoni SC. White matter development and early cognition in babies and toddlers. *Human brain mapping*. 2014;35:4475-87.

[6] Li YO, Yang FG, Nguyen CT, Cooper SR, LaHue SC, Venugopal S, Mukherjee P. Independent component analysis of DTI reveals multivariate microstructural correlations of white matter in the human brain. *Human brain mapping*. 2012;33:1431-51.

[7] Ge R, Downar J, Blumberger DM, Daskalakis ZJ, Lam RW, Vila-Rodriguez F. Structural network integrity of the central executive network is associated with the therapeutic effect of rTMS in treatment resistant depression. *Progress in Neuro-Psychopharmacology and Biological Psychiatry*. 2019;92:217-25.

[8] Kašpárek T, Mareček R, Schwarz D, Přikryl R, Vaníček J, Mikl M, Češková E. Source‐based morphometry of gray matter volume in men with first‐episode schizophrenia. *Human brain mapping*. 2010;31:300-10.

[9] Sprooten E, Gupta CN, Knowles EE, McKay DR, Mathias SR, Curran JE, Kent Jr JW, Carless MA, Almeida MA, Dyer TD. Genome‐wide significant linkage of schizophrenia‐related neuroanatomical trait to 12q24. *American Journal of Medical Genetics Part B: Neuropsychiatric Genetics*. 2015;168:678-86.

[10] Ge R, Kot P, Liu X, Lang DJ, Wang JZ, Honer WG, Vila‐Rodriguez F. Parcellation of the human hippocampus based on gray matter volume covariance: Replicable results on healthy young adults. *Human brain mapping*. 2019;40:3738-52.

[11] Ciarochi JA, Calhoun VD, Lourens S, Long JD, Johnson HJ, Bockholt HJ, Liu J, Plis SM, Paulsen JS, Turner JA. Patterns of co-occurring gray matter concentration loss across the Huntington disease prodrome. *Frontiers in neurology*. 2016;7:147.

[12] Gupta CN, Calhoun VD, Rachakonda S, Chen J, Patel V, Liu J, Segall J, Franke B, Zwiers MP, Arias-Vasquez A. Patterns of gray matter abnormalities in schizophrenia based on an international mega-analysis. *Schizophrenia bulletin*. 2015;41:1133-42.

[13] Luo N, Sui J, Abrol A, Lin D, Chen J, Vergara VM, Fu Z, Du Y, Damaraju E, Xu Y. Age‐related structural and functional variations in 5,967 individuals across the adult lifespan. *Human Brain Mapping*. 2020;41:1725-37.

[14] Mei T, Llera A, Floris DL, Forde NJ, Tillmann J, Durston S, Moessnang C, Banaschewski T, Holt RJ, Baron-Cohen S. Gray matter covariations and core symptoms of autism. The EU-AIMS Longitudinal European Autism Project. *bioRxiv*. 2020.

[15] Thompson PM, Jahanshad N, Ching CR, Salminen LE, Thomopoulos SI, Bright J, Baune BT, Bertolín S, Bralten J, Bruin WB. ENIGMA and global neuroscience: A decade of large-scale studies of the brain in health and disease across more than 40 countries. *Translational psychiatry*. 2020;10:1-28.

[16] Poldrack RA, Gorgolewski KJ. Making big data open: data sharing in neuroimaging. *Nature neuroscience*. 2014;17:1510-7.

[17] Gordon EM, Laumann TO, Gilmore AW, Newbold DJ, Greene DJ, Berg JJ, Ortega M, Hoyt-Drazen C, Gratton C, Sun H. Precision functional mapping of individual human brains. *Neuron*. 2017;95:791-807. e7.
[18] Poldrack RA. Precision neuroscience: Dense sampling of individual brains. *Neuron*. 2017;95:727-9.
[19] Calhoun VD, Adali T, Pearlson GD, Pekar JJ. A method for making group inferences from functional MRI data using independent component analysis. *Human brain mapping*. 2001;14:140-51.
[20] Erhardt EB, Rachakonda S, Bedrick EJ, Allen EA, Adali T, Calhoun VD. Comparison of multi‐subject ICA methods for analysis of fMRI data. *Human brain mapping*. 2011;32:2075-95.
[21] Erhardt EB, Allen EA, Wei Y, Eichele T, Calhoun VD. SimTB, a simulation toolbox for fMRI data under a model of spatiotemporal separability. *Neuroimage*. 2012;59:4160-7.
[22] Duan K, Chen J, Calhoun VD, Jiang W, Rootes-Murdy K, Schoenmacker G, Silva RF, Franke B, Buitelaar JK, Hoogman M. Sparse parallel independent component analysis and its application to identify linked genomic and gray matter alterations underlying working memory impairment in attention-deficit/hyperactivity disorder. *bioRxiv*. 2020.
[23] Gudbjartsson H, Patz S. The Rician distribution of noisy MRI data. *Magnetic resonance in medicine*. 1995;34:910-4.
[24] Firbank M, Coulthard A, Harrison R, Williams E. A comparison of two methods for measuring the signal to noise ratio on MR images. *Physics in Medicine & Biology*. 1999;44:N261.
[25] Magnotta VA, Friedman L, Birn F. Measurement of signal-to-noise and contrast-to-noise in the fBIRN multicenter imaging study. *Journal of digital imaging*. 2006;19:140-7.
[26] Himberg J, Hyvärinen A, Esposito F. Validating the independent components of neuroimaging time series via clustering and visualization. *Neuroimage*. 2004;22:1214-22.
[27] Pappaianni E, Siugzdaite R, Vettori S, Venuti P, Job R, Grecucci A. Three shades of grey: detecting brain abnormalities in children with autism using source‐, voxel‐and surface‐based morphometry. *European Journal of Neuroscience*. 2018;47:690-700.
[28] Turner JA, Calhoun VD, Michael A, Van Erp TG, Ehrlich S, Segall JM, Gollub RL, Csernansky J, Potkin SG, Ho B-C. Heritability of multivariate gray matter measures in schizophrenia. *Twin Research and Human Genetics*. 2012;15:324-35.
[29] Wolf RC, Huber M, Lepping P, Sambataro F, Depping MS, Karner M, Freudenmann RW. Source-based morphometry reveals distinct patterns of aberrant brain volume in delusional infestation. *Progress in Neuro-Psychopharmacology and Biological Psychiatry*. 2014;48:112-6.
[30] Correa N, Adalı T, Calhoun VD. Performance of blind source separation algorithms for fMRI analysis using a group ICA method. *Magnetic resonance imaging*. 2007;25:684-94.
[31] Chen J, Liu J, Calhoun VD, Arias-Vasquez A, Zwiers MP, Gupta CN, Franke B, Turner JA. Exploration of scanning effects in multi-site structural MRI studies. *Journal of neuroscience methods*. 2014;230:37-50.
[32] Li H, Smith SM, Gruber S, Lukas SE, Silveri MM, Hill KP, Killgore WD, Nickerson LD. Denoising scanner effects from multimodal MRI data using linked independent component analysis. *NeuroImage*. 2020;208:116388.
[33] Tijms BM, Seriès P, Willshaw DJ, Lawrie SM. Similarity-based extraction of individual networks from gray matter MRI scans. *Cerebral cortex*. 2012;22:1530-41.

FIGURE LEGENDS

Fig 1. Flowcharts of the two analysis strategies of source-based morphometry (SBM). PCA: principal component analysis. **X**, **A**, and **S** indicate the MRI data matrix, loading parameter matrix, and spatial structural brain pattern (SBP) matrix. The MRI data matrix can be a matrix of gray matter volume, cortical thickness, or fractional anisotropy etc.

Fig 2. (**A**) Spatial locations of the simulated structural brain patterns; the first 10 data were comprised of 15 patterns (pattern IDs: 1-15), and the second 10 data were comprised of 15 patterns (pattern IDs: 1-14, and 16). Whole-sample-level results of the conventional analysis strategy (**B**) and SS-Detect analysis strategy (**C**). (**D**) Individualized scanner-specific results of the first 10 data and the second 10 data. A one-sample t-test was used to summarize the first 10 data and second 10 data separately.

Fig 3. (**A**) Average Dice's coefficient between the 16 structural brain patterns (SBPs) and the ground truth at the whole-sample-level. Statistical analysis showed that the estimated SBPs from the SS-Detect analysis strategy had higher AUC and Dice's coefficient (at z-score of 2.5) relative to the conventional analysis strategy. (**B**) Average Dice's coefficient between the 15 SBPs and the spatial ground truth at the individual scanner-level for the first and second 10 simulated data, respectively. (**C**) Average correlation coefficient between the estimated loading parameters and the ground truth for the first and second 10 simulated data, respectively. Error bars indicate the standard error across all SBPs. AUC: area under curve.

Fig 4. (**A**) Spatial location of the simulated component. Whole-sample-level results of the conventional analysis strategy (**B**) and SS-Detect analysis strategy (**C**). (**D**) Individualized scanner-specific results. A one-sample t-test was used to summarize the results of Philips and GE data separately.

Fig 5. (**A**) Average Dice's coefficient between the simulated structural brain pattern (SBP) and the ground truth at the whole-sample-level. Statistical analysis showed that the estimated SBP from the SS-Detect analysis strategy had higher AUC and Dice's coefficient (at z-score of 2.5) relative to the conventional analysis strategy. (**B**) Average Dice's coefficient between the estimated SBP and the spatial ground truth at the individual scanner-level for the Philips and GE data, respectively. (**C**) Average correlation coefficient between the loading parameters and the ground truth for the Philips and GE data, respectively. Error bars indicate the standard error across the 10 repetitions of the simulation. AUC: area under curve.

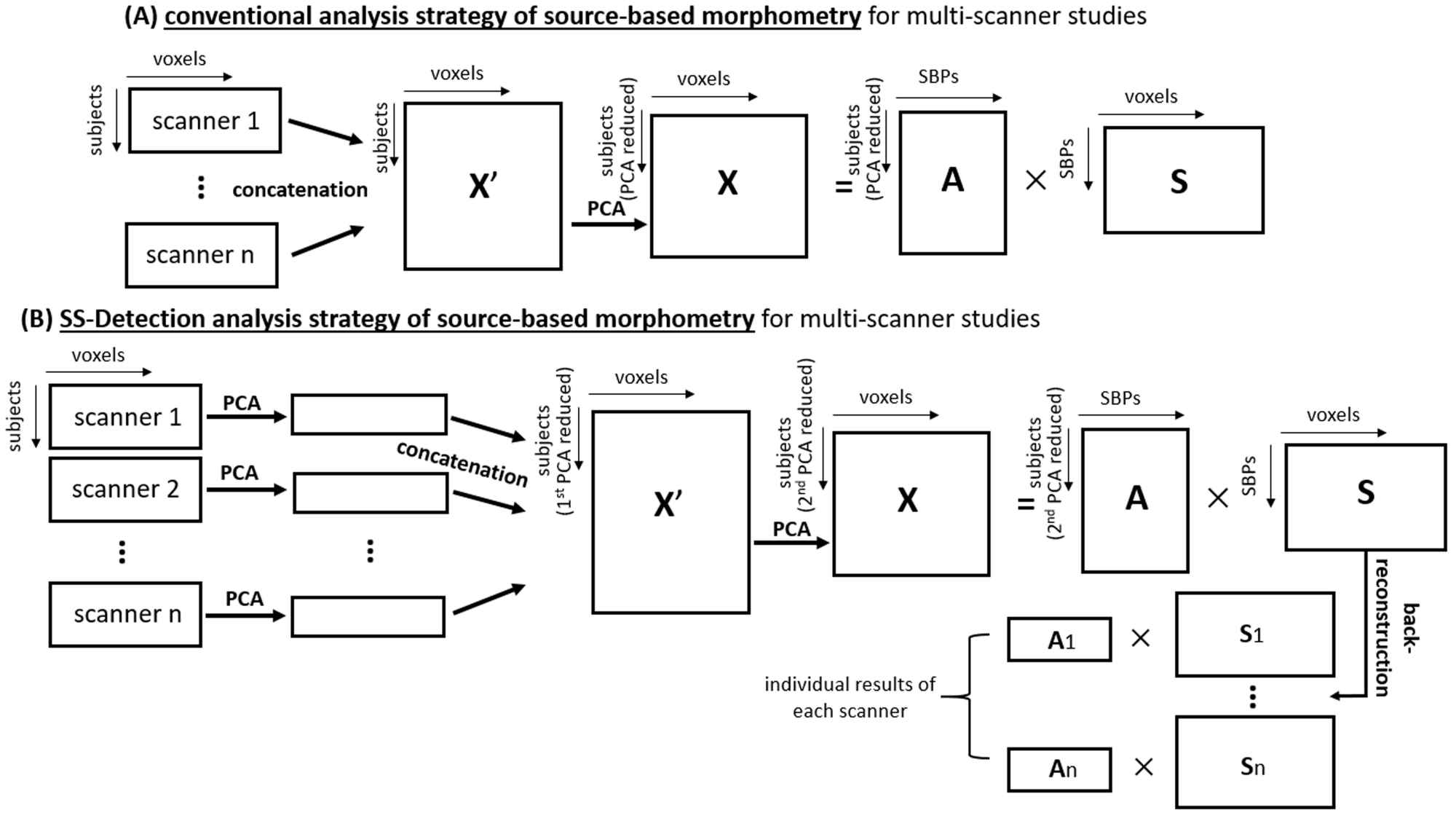
(A) conventional analysis strategy of source-based morphometry for multi-scanner studies
voxels
subjects
scanner 1
concatenation
scanner n
X'
PCA
subjects (PCA reduced)
X
=
A
SBPs
×
S
(B) SS-Detection analysis strategy of source-based morphometry for multi-scanner studies
scanner 2
PCA
subjects (1st PCA reduced)
subjects (2nd PCA reduced)
individual results of each scanner
A1
S1
An
Sn
back-reconstruction

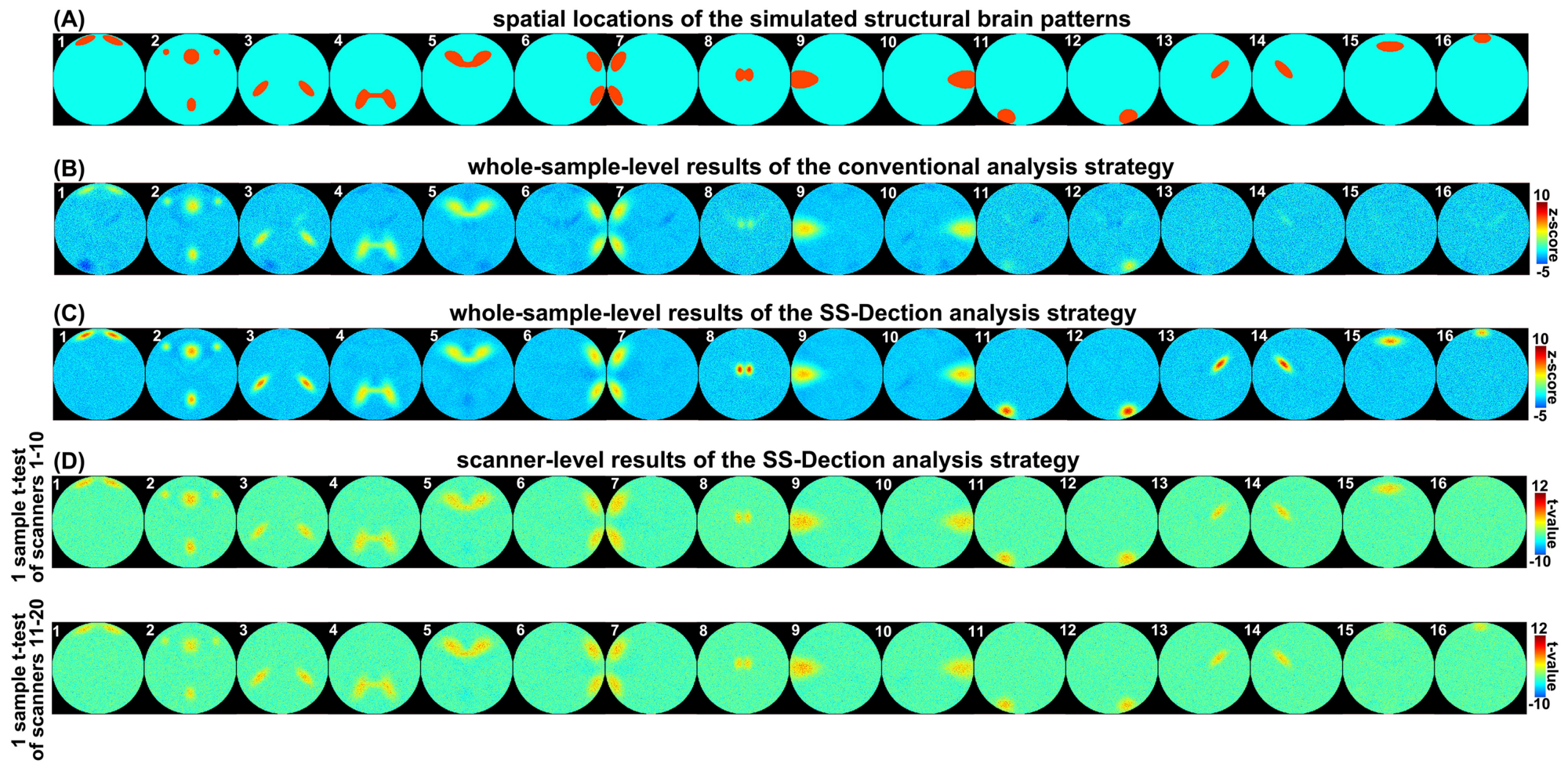
(A)
spatial locations of the simulated structural brain patterns
1
2
3
4
5
6
7
8
9
10
11
12
13
14
15
16
(B)
whole-sample-level results of the conventional analysis strategy
10
z-score
-5
(C)
whole-sample-level results of the SS-Dection analysis strategy
10
z-score
-5
(D)
scanner-level results of the SS-Dection analysis strategy
1 sample t-test of scanners 1-10
12
t-value
-10
1 sample t-test of scanners 11-20
12
t-value
-10

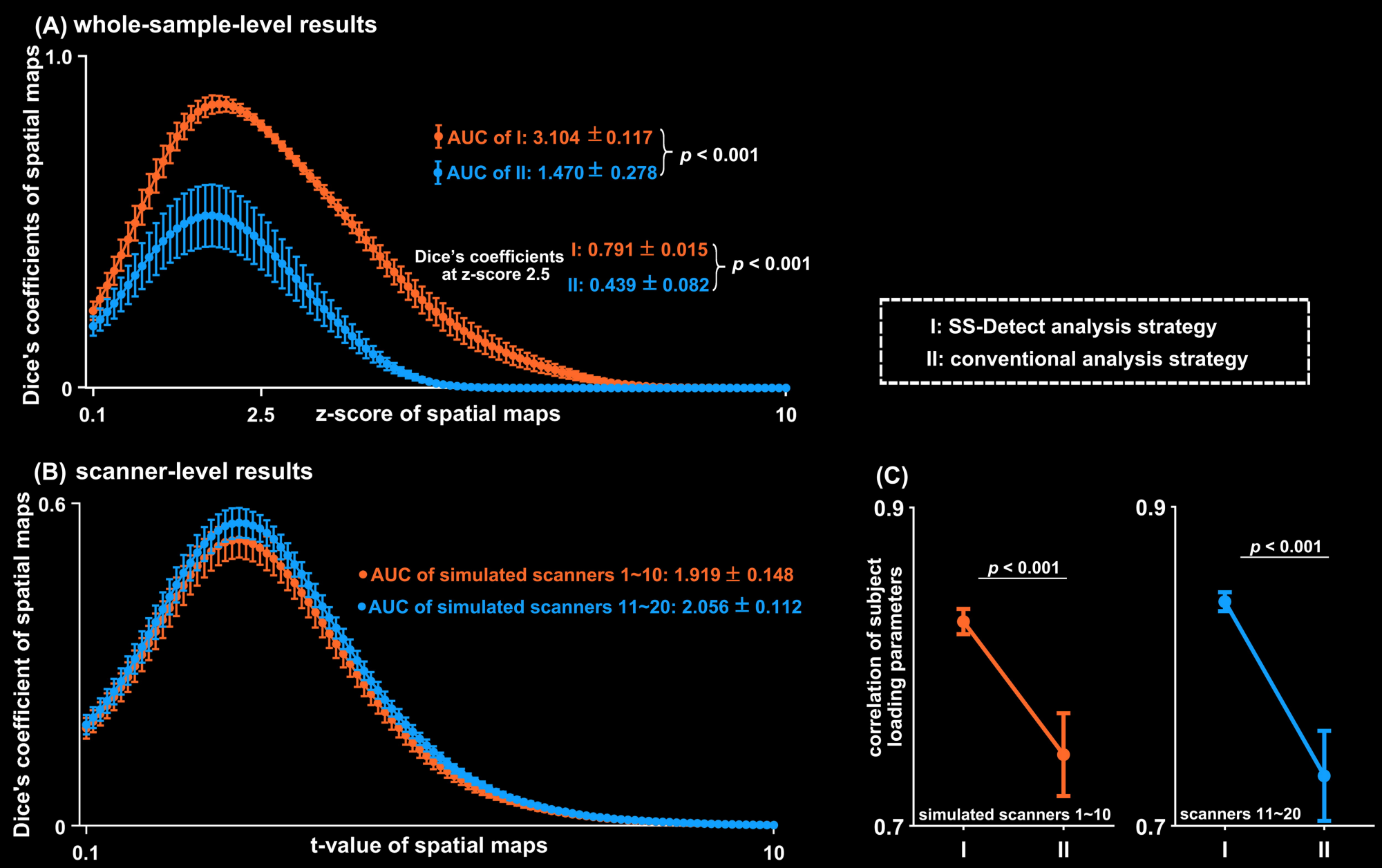
(A) whole-sample-level results
Dice's coefficients of spatial maps
1.0
0
0.1
2.5
z-score of spatial maps
10
AUC of I: 3.104 ± 0.117
AUC of II: 1.470 ± 0.278
p < 0.001
Dice's coefficients at z-score 2.5
I: 0.791 ± 0.015
II: 0.439 ± 0.082
p < 0.001
I: SS-Detect analysis strategy
II: conventional analysis strategy
(B) scanner-level results
Dice's coefficient of spatial maps
0.6
0
0.1
t-value of spatial maps
10
AUC of simulated scanners 1~10: 1.919 ± 0.148
AUC of simulated scanners 11~20: 2.056 ± 0.112
(C)
correlation of subject loading parameters
0.9
0.7
p < 0.001
simulated scanners 1~10
I
II
0.9
0.7
p < 0.001
scanners 11~20
I
II

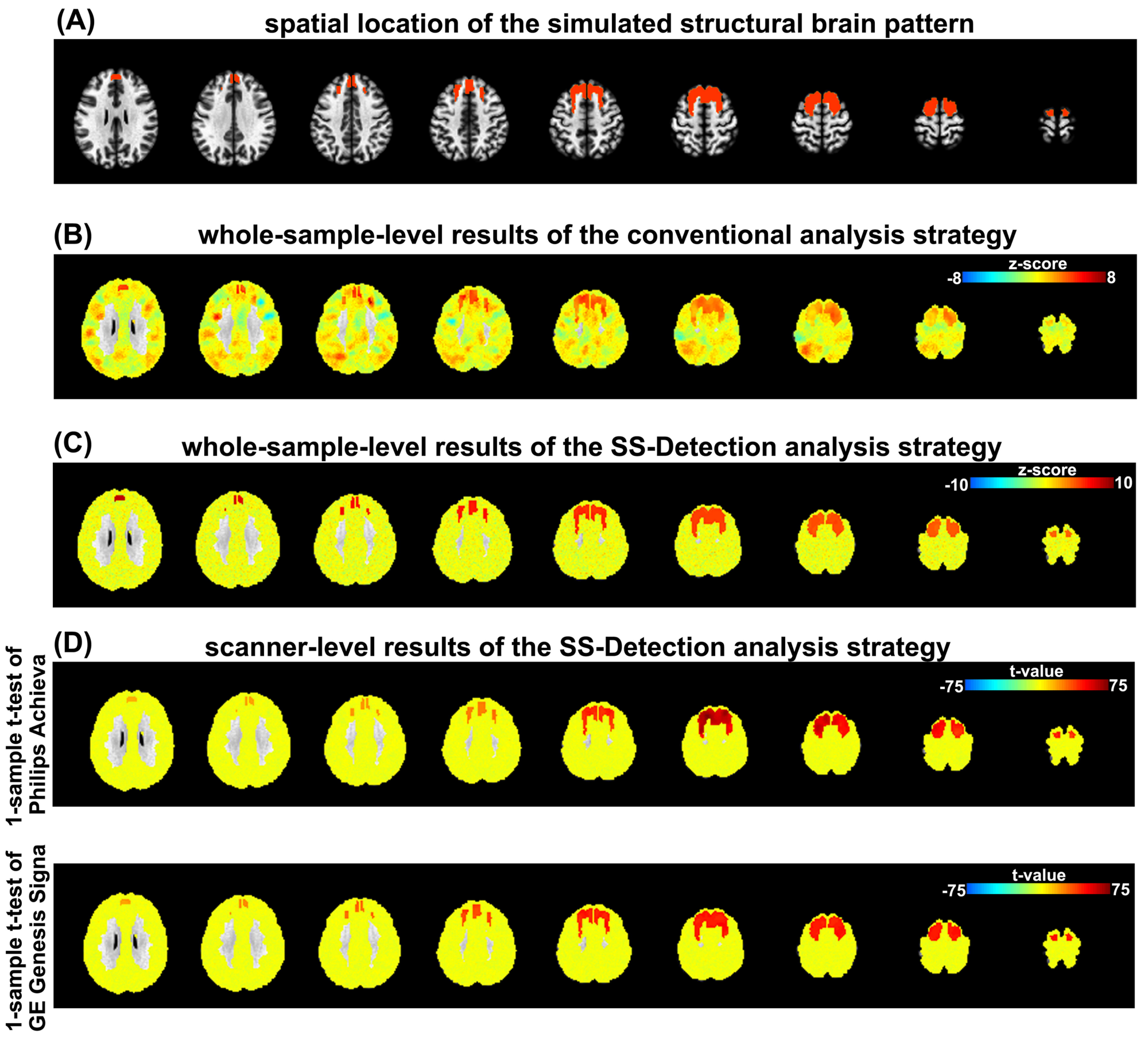
(A)
spatial location of the simulated structural brain pattern
(B)
whole-sample-level results of the conventional analysis strategy
z-score
-8
8
(C)
whole-sample-level results of the SS-Detection analysis strategy
z-score
-10
10
(D)
scanner-level results of the SS-Detection analysis strategy
1-sample t-test of Philips Achieva
t-value
-75
75
1-sample t-test of GE Genesis Signa
t-value
-75
75

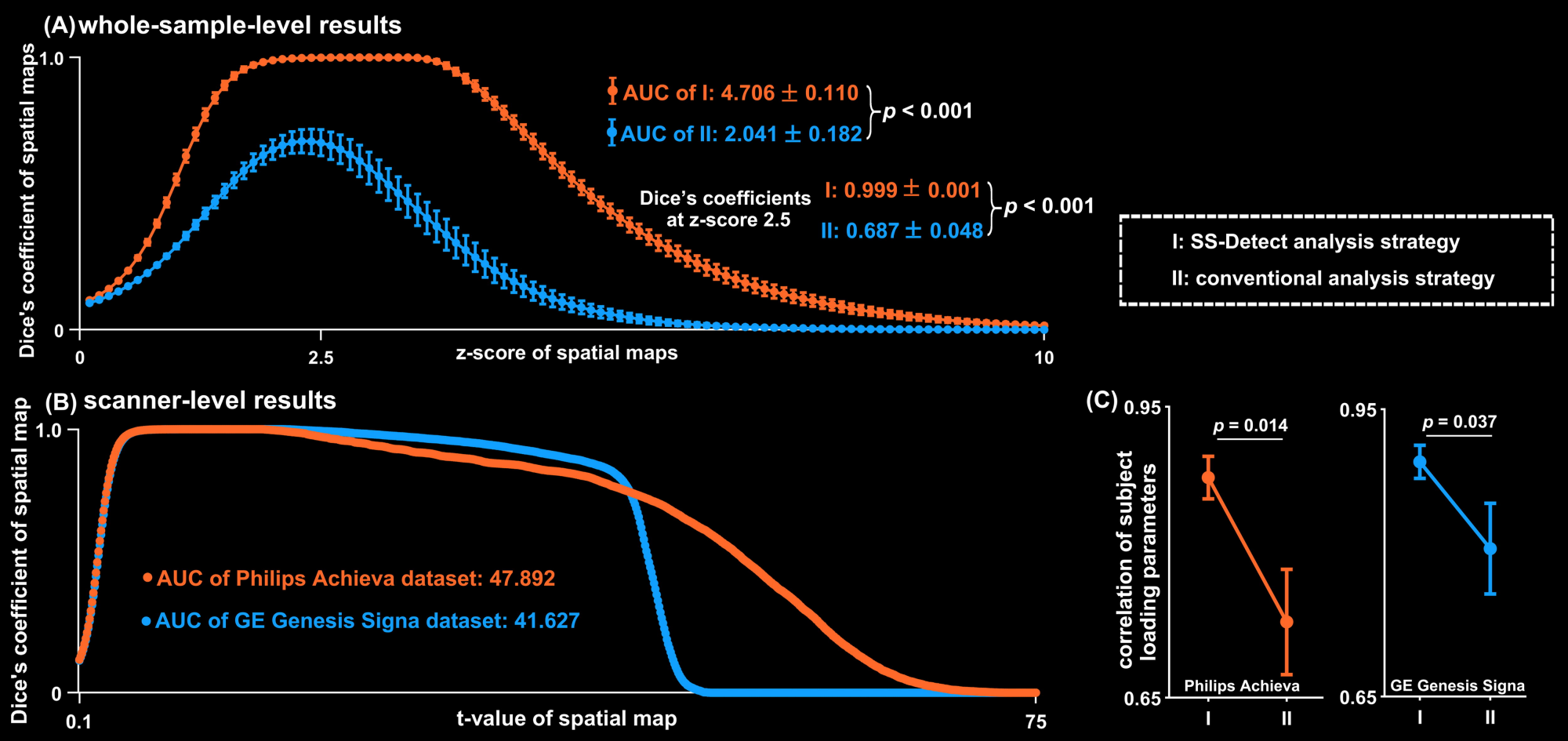
(A) whole-sample-level results
Dice's coefficient of spatial maps
1.0
0
0
2.5
10
z-score of spatial maps
AUC of I: 4.706 ± 0.110
AUC of II: 2.041 ± 0.182
p < 0.001
Dice's coefficients at z-score 2.5
I: 0.999 ± 0.001
II: 0.687 ± 0.048
p < 0.001
I: SS-Detect analysis strategy
II: conventional analysis strategy
(B) scanner-level results
Dice's coefficient of spatial map
1.0
0
0.1
75
t-value of spatial map
AUC of Philips Achieva dataset: 47.892
AUC of GE Genesis Signa dataset: 41.627
(C)
correlation of subject loading parameters
0.95
0.65
p = 0.014
Philips Achieva
I
II
p = 0.037
GE Genesis Signa